PNAS PLUS

miR-285–Yki/Mask double-negative feedback loop mediates blood–brain barrier integrity in *Drosophila*

Dong Li[a,b], Yanling Liu[a,b], Chunli Pei[c,d], Peng Zhang[c,d], Linqing Pan[a,b], Jing Xiao[e], Songshu Meng[b], Zengqiang Yuan[c,d,1], and Xiaolin Bi[a,b,1]

[a]Department of Biological Sciences, College of Basic Medical Sciences, Dalian Medical University, Dalian 116044, China; [b]Institute of Cancer Stem Cell, Cancer Center, Dalian Medical University, Dalian 116044, China; [c]The Brain Science Center, Beijing Institute of Basic Medical Sciences, Beijing 100850, China; [d]Center of Alzheimer's Disease, Beijing Institute for Brain Disorders, Beijing 100069, China; and [e]Department of Oral Basic Science, College of Stomatology, Dalian Medical University, Dalian 116044, China

Edited by Norbert Perrimon, Harvard Medical School/HHMI, Boston, MA, and approved February 10, 2017 (received for review August 9, 2016)

The Hippo signaling pathway is highly conserved from *Drosophila* to mammals and plays a central role in maintaining organ size and tissue homeostasis. The blood–brain barrier (BBB) physiologically isolates the brain from circulating blood or the hemolymph system, and its integrity is strictly maintained to perform sophisticated neuronal functions. Until now, the underlying mechanisms of subperineurial glia (SPG) growth and BBB maintenance during development are not clear. Here, we report an *miR-285*–Yorkie (Yki)/Multiple Ankyrin repeats Single KH domain (Mask) double-negative feedback loop that regulates SPG growth and BBB integrity. Flies with a loss of *miR-285* have a defective BBB with increased SPG ploidy and disruptive septate junctions. Mechanistically, *miR-285* directly targets the Yki cofactor Mask to suppress Yki activity and down-regulates the expression of its downstream target *cyclin E*, a key regulator of cell cycle. Disturbance of *cyclin E* expression in SPG causes abnormal endoreplication, which leads to aberrant DNA ploidy and defective septate junctions. Moreover, the expression of *miR-285* is increased by knockdown of *yki* or *mask* and is decreased with *yki* overexpression, thus forming a double-negative feedback loop. This regulatory loop is crucial for sustaining an appropriate Yki/Mask activity and *cyclin E* level to maintain SPG ploidy and BBB integrity. Perturbation of this signaling loop, either by dysregulated *miR-285* expression or Yki activity, causes irregular SPG ploidy and BBB disruption. Furthermore, ectopic expression of *miR-285* promotes canonical Hippo pathway-mediated apoptosis independent of the p53 or JNK pathway. Collectively, these results reveal an exquisite regulatory mechanism for BBB maintenance through an *miR-285*–Yki/Mask regulatory circuit.

Hippo | Mask | *miR-285* | blood–brain barrier | subperineurial glia

To efficiently perform sophisticated neuronal functions, a well-balanced ion influx and efflux, as well as a steady supply of metabolites and nutrients, is required by the nervous system. To maintain the homeostasis of ions and metabolites and prevent the transport of neurotoxins and pathogens into the brain, the highly selective and permeable barrier called the blood–brain barrier (BBB) is evolutionarily conserved from invertebrates to vertebrates. The primitive BBB is formed at the embryonic stage and continues to mature after birth. In higher order vertebrates, the BBB is formed primarily by the brain vascular endothelium (1, 2); however, in *Drosophila*, the BBB is formed by two distinct classes of glial cells, perineurial glia (PG) and subperineurial glia (SPG). The apical PG cells form the first barrier to prevent diffusion, and basal SPG cells form the extensive septate junctions, a form of tight junctions, to prevent paracellular diffusion and are considered the structural basis of the BBB (3, 4).

PG cells in *Drosophila* are not required to form the BBB during early development, whereas SPG cells are essential for BBB maintenance during the early developmental stage and throughout development to the adult stage (5). SPG cells form a flat, continuous layer and tightly seal around the entire nervous system, and their proliferation is restricted to embryogenesis (5, 6). During the larval stage, no additional SPG cells are generated, with the animals growing to a much larger size; thus, SPG cells from the embryonic stage grow enormously in size to maintain integrity of the BBB (7). Although an increased cell size can be achieved through the accumulation of cell mass during the growth of diploid cells, cell size is often correlated with the ploidy of DNA content and is increased via polyploidy during development, characteristics that are important for organogenesis, such as proper organ size, structure, and function (8–10). SPG cells have been shown to maintain the integrity of the BBB during development by increased ploidy with increased cell size (7). Despite its critical role in BBB formation and maintenance, the underlying mechanisms regulating SPG cell growth and polyploidy are still poorly understood.

Previous studies have shown that Wnt/β-catenin and Sonic Hedgehog (SHH) signaling pathways are essential for BBB integrity (11). In *Drosophila*, Decapentaplegic (Dpp)/TGF-β, Hedgehog (Hh), and EGFR pathways promote proliferation and motility of glial cells (12, 13). The coactivation of EGFR and PI3K signaling pathways in glia induces neoplasia (14). Recently, Yorkie (Yki), a major effector of the Hippo pathway that regulates growth control, was reported to regulate proliferation of glial cells (15). Originally identified in *Drosophila* and highly conserved from *Drosophila* to mammals, the Hippo signaling pathway plays a central role in regulating organ size and tissue homeostasis. Central to this pathway is a kinase cascade leading from Hippo to Yki (YAP and TAZ in mammals), ultimately inactivating Yki through phosphorylation and sequestering its subcellular localization from cytoplasm to nucleus. In response to different intracellular or extracellular stimuli, the Hippo pathway regulates cell proliferation, apoptosis, and stemness (16).

Significance

The blood–brain barrier (BBB) is evolutionarily conserved from invertebrates to vertebrates to ensure a well-balanced ionic environment for proper neuronal functions. The Hippo pathway is a highly conserved signaling pathway essential for organ size control and tissue homeostasis. Until now, whether Hippo pathway is required for BBB maintenance has been unknown. We show here that *miR-285* is an upstream regulator of the Hippo pathway, which can directly target Yorkie (Yki) cofactor Multiple Ankyrin repeats Single KH domain (Mask). *miR-285* and Yki/Mask form a double-negative feedback loop to finely tune endoreplication of subperineurial glial (SPG) cells to keep proper cell size and maintain a functional BBB. Our findings propose an exquisite microRNA-mediated regulatory circuit that regulates Hippo signaling activity and tissue homeostasis during development.

Author contributions: D.L., Z.Y., and X.B. designed research; D.L., Y.L., C.P., and L.P. performed research; P.Z., J.X., S.M., and Z.Y. contributed new reagents/analytic tools; D.L. and X.B. analyzed data; and D.L. and X.B. wrote the paper.

The authors declare no conflict of interest.

This article is a PNAS Direct Submission.

[1]To whom correspondence may be addressed. Email: bixl@dmu.edu.cn or zyuan620@yahoo.com.

This article contains supporting information online at www.pnas.org/lookup/suppl/doi:10.1073/pnas.1613233114/-/DCSupplemental.

As a transcription coactivator, Yki works with its major partner, Sd, in flies to regulate the expression of global genes. Multiple Ankyrin repeats Single KH domain (MASK) protein is a newly identified cofactor of Yki in *Drosophila*. By forming a complex with Yki and Sd, Mask regulates cell proliferation and tissue growth through positively modulating Yki activity and its downstream gene expression (17, 18). YAP/TAZ can also regulate microRNA biogenesis in a cell density-dependent manner through modulation of microRNA processing enzymes Microprocessor or Dicer complexes (16, 19–21). In *Drosophila*, the microRNA *bantam* is a downstream target of Yki and is required for Yki-regulated cell growth (22, 23). *bantam* represses the Yki inhibitor SdBP/Tgi to establish a feedback loop, which functionally mimics its mammalian homolog *miR-130a* targeting VGLL4, a YAP inhibitor (24). Although the core signaling cascade of the Hippo pathway has been extensively studied, whether Hippo pathway is functional at BBB maintenance is unknown, and the regulatory mechanisms underlying Hippo signaling are key questions that remain unanswered in the Hippo research field.

In this study, we report that *Drosophila miR-285* regulates BBB integrity via the Hippo signaling pathway. Flies with a loss of *miR-285* exhibit disrupted septate junctions and defective BBB. *miR-285* directly targets Yki cofactor Mask, and SPG cells in *miR-285*^{KO} flies have enhanced Yki activity and *cyclin E* expression, which leads to increased DNA ploidy, nuclear size in SPG cells, and brain hemisphere volume. These defects can be almost fully rescued with the restricted expression of *miR-285* or knockdown of *mask* or *cyclin E* expression. Furthermore, Yki/Mask forms a double-negative feedback loop with *miR-285* that is required for fine-tuning the DNA content in SPG during development. Thus, we provide direct evidence that the Hippo signaling pathway is required for BBB integrity and identify an elaborate mechanism for BBB maintenance via the *miR-285*–Yki/Mask feedback signaling loop, which is critical for the exquisite regulation of SPG polyploidy.

Results

***miR-285* Is a Regulator of the Hippo Pathway by Targeting Mask.** To explore the regulatory mechanisms of the Hippo signaling pathway, we generated *tubulin-EGFP* sensor lines containing the 3′UTRs of *mask*, *sd*, or *ex*, which are components of the Hippo pathway (16), and performed gain-of-expression screening for microRNAs that

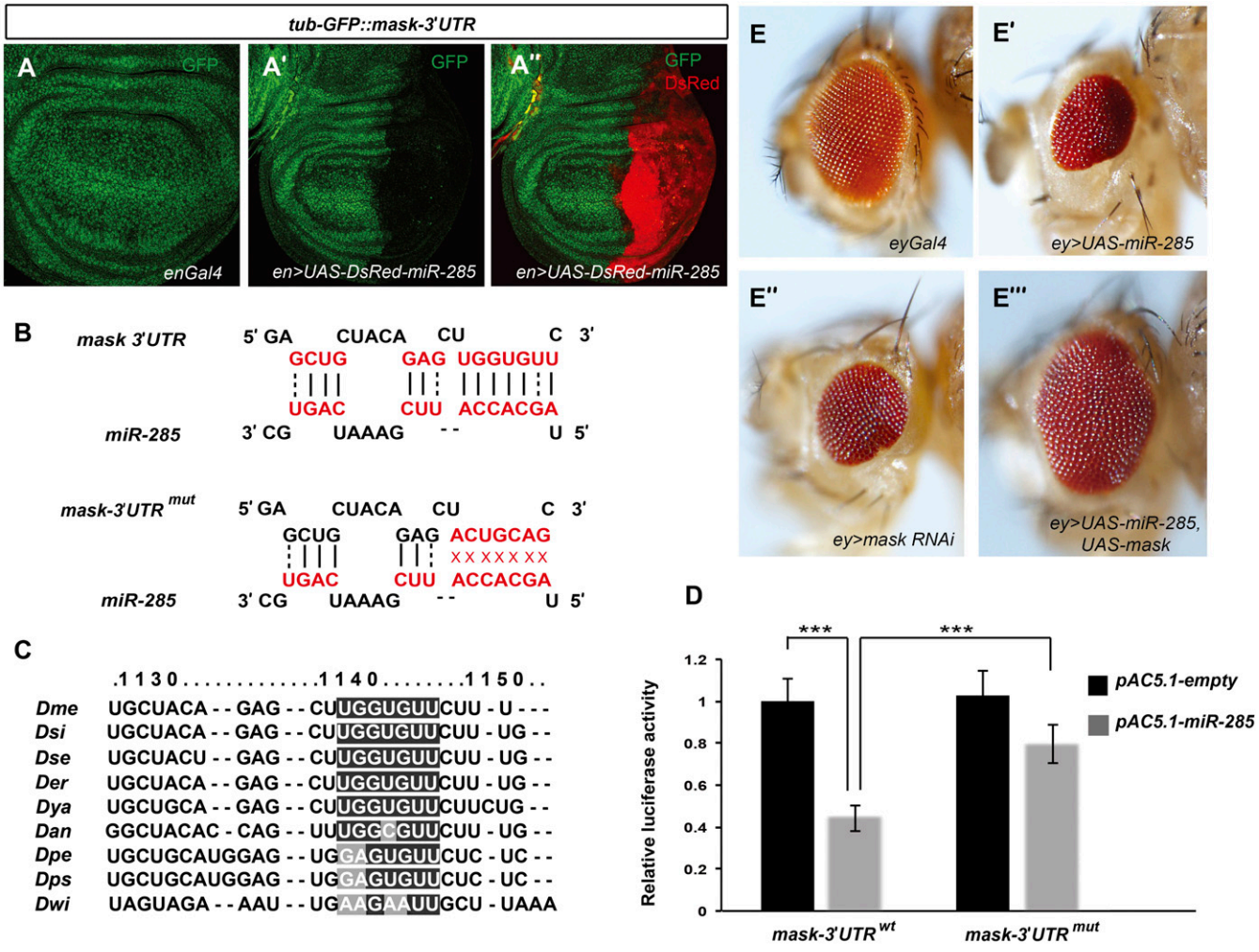

Fig. 1. *miR-285* directly targets *mask*. (*A*–*A″*) Wing discs showing expression of GFP in a *tub-GFP::mask 3′UTR* sensor (*A*) in *miR-285* overexpression driven by *en-Gal4* (*A′*) and overlapping (*A″*). (*B*) Predicted targeting site for *miR-285* in *mask* 3′UTR. Seed sequence and mutagenesis of the seed sequence in *mask* 3′UTR are shown in red. (*C*) Sequence alignment of *miR-285* targeting site in *mask 3′UTR* among *Drosophila* species. The conserved sequence is highlighted in black. (*D*) Luciferase assay. S2 cells were transfected with *pAC5.1-miR-285* or *pAC5.1-empty*, together with a firefly luciferase vector containing *mask* 3′UTR (*mask-3′UTR*^{wt}) or the *miR-285* targeting site mutated *mask* 3′UTR (*mask-3′UTR*^{mut}). The data shown are means ± SEM from three experiments. The *P* value was noted as follows: ***$P < 0.001$. (*E*–*E‴*) Overexpression of *miR-285* and knockdown of *mask* driven by *ey-Gal4* resulted in small eyes (*E′* and *E″*), and overexpression of *mask* suppressed the small eye phenotype caused by *miR-285* overexpression (*E‴*).

can target the Hippo pathway. Overexpression of *miR-285* driven by *engrailed* (*en*)-*Gal4* in vivo decreased the expression of *tub-EGFP-sensor* containing *mask* 3′UTR specifically in the posterior compartment of wing discs (Fig. 1 *A′* and *A″*), suggesting that *miR-285* could regulate the Hippo pathway through Mask, a newly identified Yki cofactor (17, 18). Bioinformatic analysis using miRanda software suggested a putative targeting site for *miR-285* in *mask* 3′UTR (Fig. 1*B*), which is a noncanonical *miR-285* targeting site with one G:U wobble pairing in the seed region. Although this site is conserved among *Drosophila melanogaster* subgroup species, it is poorly conserved among *Drosophila* species (Fig. 1*C*), indicating that it is a newly evolved targeting site of *miR-285*. To prove that *miR-285* binding to *mask* depends on this site, a complementary sequence to the *miR-285* seed in the *mask* 3′UTR was mutated to abolish potential *miR-285* binding (Fig. 1*B*). By performing a luciferase assay in *Drosophila* Schneider S2 cells, we found that reporter containing wild-type *mask* 3′UTR had reduced luciferase activity by 55% with *miR-285* coexpression compared with that in control cells, suggesting that *miR-285* can also target *mask* in vitro ($P < 0.001$; Fig. 1*D*). Luciferase activity was recovered when the reporter containing mutated *mask* 3′UTR was cotransfected with the *miR-285* construct ($P < 0.001$; Fig. 1*D*). Furthermore, overexpression of *miR-285* driven by *ey-Gal4* induced the small eye phenotype, which was phenocopied by knockdown of *mask* by RNAi (Fig. 1 *E–E″*). The overexpression of *mask* rescued the eye phenotype caused by *miR-285* overexpression (Fig. 1*E‴*), providing additional evidence that *mask* is a downstream target of *miR-285*. Together, we identified *miR-285* as a regulator of the Hippo pathway through targeting *mask*.

***miR-285* Is Essential for BBB Integrity.** Cytogenetically, *miR-285* is located on the third chromosome as an intergenic microRNA (Fig. 2*A*). To study its physiological functions, we detected its expression at the third instar larval stage (L3) using in situ hybridization (ISH). Highly expressed *miR-285* was observed in brains from wild-type flies (Fig. 2*B*), whereas it was undetectable in the salivary gland, eye disk, leg disk, gut (Fig. S1 *A–D*), and wing disk (anterior compartment, arrowhead in Fig. S1*F*). Furthermore, *miR-285* expression could be seen in the posterior compartment of the wing disk (star in Fig. S1*F*) with enforced expression driven by *hh-Gal4*; however, a much more abundant signal was detected in brains driven by the pan-glial driver *repo-Gal4* (Fig. S1*E*). Genome-wide microRNA knockout flies were recently established by targeted homologous recombination (25), in which *miR-285* was

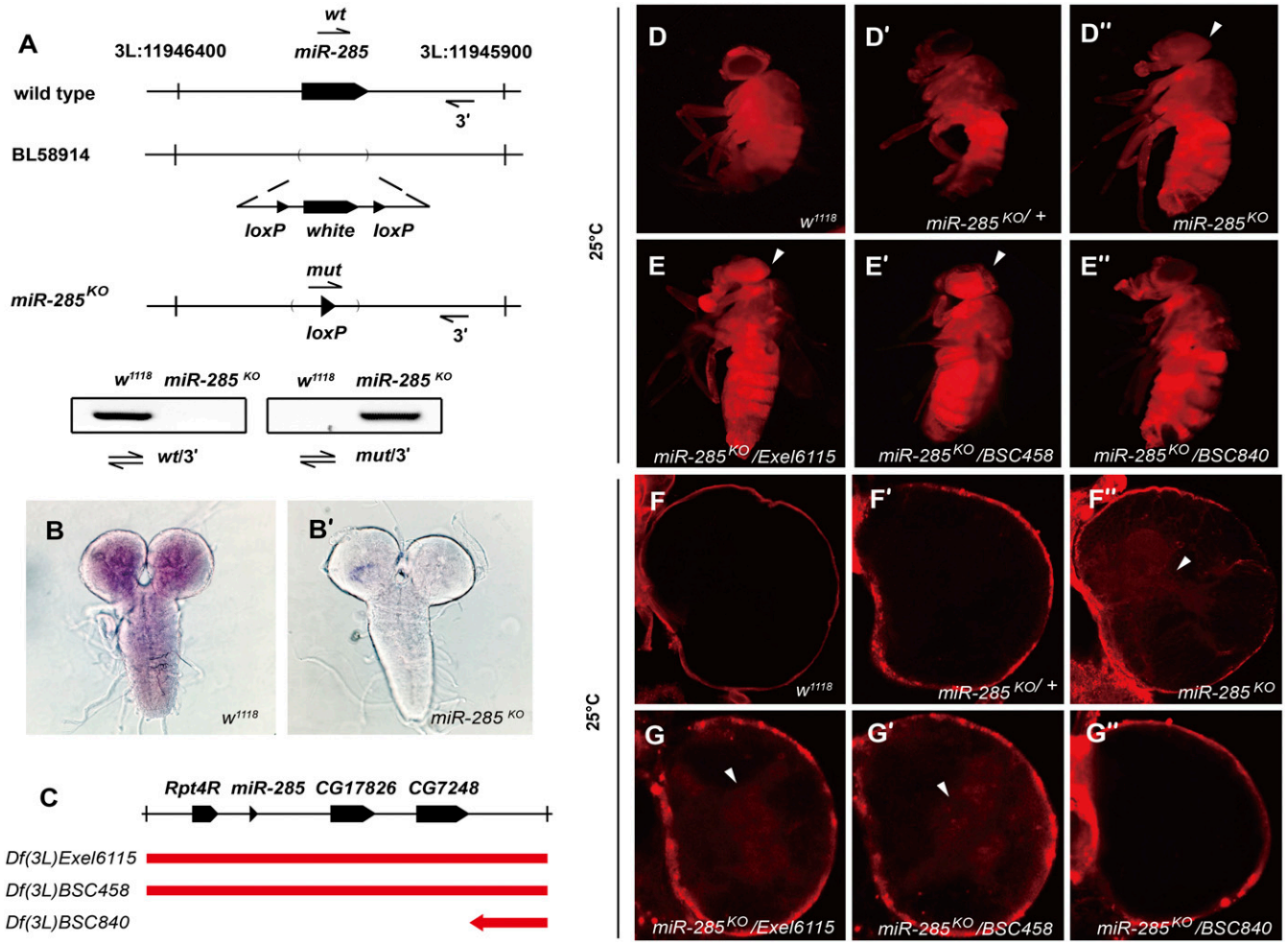

Fig. 2. *miR-285* is essential for a functional BBB. (*A*) Genomic organization of the *miR-285* region. The miniwhite gene in BL58914 flies was removed by Cre-mediated recombination of LoxP sites to generate *miR-285*^{KO} flies. PCR was performed to verify the loss of *miR-285* gene. (*B* and *B′*) De novo expression of *miR-285* in third instar larval brains of wild-type (*B*) and *miR-285*^{KO} flies (*B′*) was revealed by LNA-probe ISH. (*C*) Scheme of deficiency lines. The red bars indicate the deleted chromosomal region for each deficiency line. (*D–D″* and *E–E″*) Dye penetration into the eye of adults was observed in *miR-285* homozygous mutant and over deficiency lines (arrowheads). (*F–F″* and *G–G″*) Dye penetration into the brain of third instar larvae was observed in *miR-285* homozygous mutant and over deficiency lines (arrowheads).

replaced by a miniwhite gene flanked by LoxP sites (Fig. 2*A*). To exclude the possible influence of ectopic expression by an inserted gene, the miniwhite gene in the BL58914 line was excised by Cre-mediated recombination of LoxP sites to generate an *miR-285*–null allele, with further verification by PCR (Fig. 2*A*), ISH (Fig. 2*B′*), and sequencing. We referred to this allele as *miR-285^{KO}* and used it in subsequent studies.

Homozygous *miR-285^{KO}* flies were viable, fertile, and had no obvious developmental defect when raised under normal conditions. A previous systemic study has suggested that *miR-285* is one of the microRNAs for which targeted deletion could cause disrupted integrity of the BBB (25). Consistent with this study, we observed compromised BBB in *miR-285^{KO}* flies when fluorescent dye Texas red-conjugated dextran was injected into the body cavity of L3 larvae or adults. Injected adults or larvae of *miR-285^{KO}* flies showed dye diffusion into adult retinas or larval brains (Fig. 2 *D″* and *F″*), whereas fluorescent dye failed to penetrate into retinas or larval brains, and a narrow rim of fluorescence was observed surrounding the retina or edge of brain lobes in wild-type flies (Fig. 2 *D* and *F*). To provide further evidence that the compromised BBB was caused by loss of *miR-285*, two *miR-285*–deficiency lines, *Df(3L)Exel6115* and *Df(3L)BSC458*, were crossed to *miR-285^{KO}* flies; however, *Df(3L)BSC840*, in which *miR-285* was not deleted, was used as the control (Fig. 2*C*). Transheterozygous *miR-285^{KO}/Df(3L)Exel6115* and *miR-285^{KO}/Df(3L)BSC458* flies displayed a disrupted BBB as homozygous *miR-285^{KO}* flies, whereas *miR-285$^{KO/+}$* and *miR-285^{KO}/Df(3L)BSC840* flies exhibited a functional BBB as wild-type flies (Fig. 2 *D–D″*, *E–E″*, *F–F″*, and *G–G″*). Therefore, a dysfunctional BBB phenotype in *miR-285^{KO}* flies is due to the loss of *miR-285*. Interestingly, the overexpression of *miR-285* driven by SPG-specific *moody-Gal4* (26, 27) at 25 °C caused a more severe BBB defect than that of *miR-285^{KO}* flies (Fig. S2 *C″* and *D″* and Table S1) and a less severe defect at 18 °C (Fig. 3 *C–C″* and Table S1), suggesting that not only *miR-285* but also its correct expression level is required for the maintenance of a functional BBB.

Next, we tested whether the BBB defect in *miR-285^{KO}* flies can be rescued by *miR-285* expression. As Gal4 activity is temperature sensitive (28), flies growing at 18 °C will have a lower level expression of the transgene than those grown at 25 °C. Flies were raised at 18 °C for an optimized rescue assay, and the BBB defect in *miR-285^{KO}* L3 flies was almost fully rescued with the restricted expression of *miR-285* in SPG cells (Fig. 3*D″*) and was largely rescued in *miR-285^{KO}* adults (Fig. 3*D‴*). To rate the severity of the BBB defect in adults, the permeability was scaled from – to +++ by scoring the intensity of the fluorescent signals in injected adult flies (Fig. S3) (29). The BBB defect was comparable in *miR-285^{KO}* flies raised under two temperatures (permeability +++, 30% at 18 °C vs. 34% at 25 °C; $n = 50$; Table S1), whereas the restricted expression of *miR-285* at 18 °C dramatically rescued the BBB defect in *miR-285^{KO}* flies (permeability +, 70%; +++, 0%; $n = 30$; Table S1). By contrast, expression of *miR-285* at 25 °C could not rescue the BBB defect (permeability +++, 83.3%; $n = 30$; Table S1). These results suggested that the appropriate expression level of *miR-285* is critical for the maintenance of a functional BBB during development.

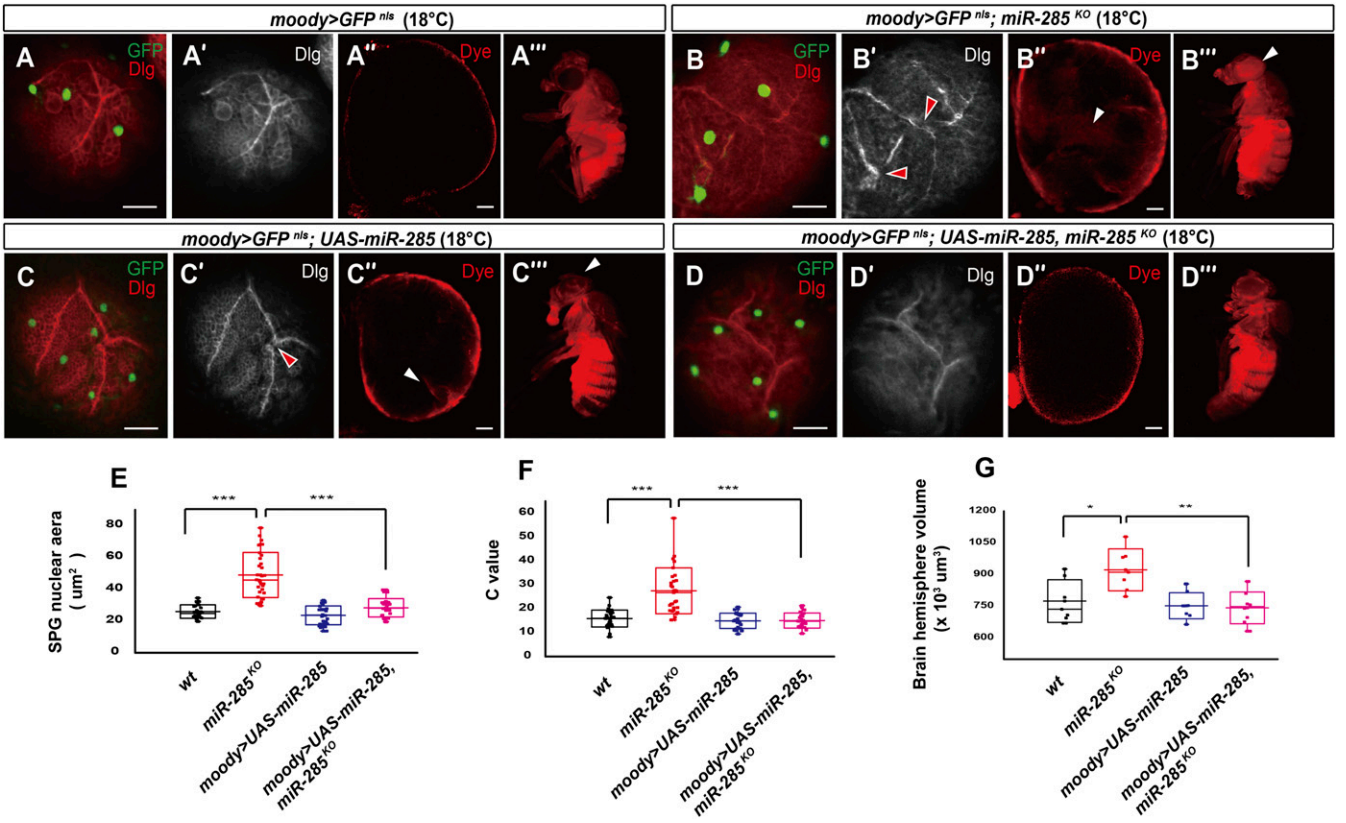

Fig. 3. *miR-285* regulates SPG ploidy and BBB integrity. Third instar larval brain lobes were collected from control (*A–A‴*), *miR-285^{KO}* (*B–B‴*), *moody* > *UAS-miR-285* (*C–C‴*), and *moody* > *UAS-miR-285*, *miR-285^{KO}* (*D–D‴*) flies raised at 18 °C. SPG nuclei were labeled with *moody* > *UAS-GFP^{nls}*, and pattern of septate junctions was shown by Dlg antibody staining. The arrowheads indicate disrupted septate junctions and dye penetration. (*E*) Quantification of the SPG nuclei size of indicated genotypes (SPG nuclei $n = 30$, from 10 larval brains). (*F*) Quantification of the polyploidy of indicated genotypes (SPG nuclei $n = 30$, from 10 larval brains). (*G*) Quantification of the brain hemisphere volume of indicated genotypes ($n = 7$). The data shown are means ± SEM, and *P* value was noted as follows: $*P < 0.05$, $**P < 0.01$, $***P < 0.001$. (Scale bar, 25 μm.)

Loss of *miR-285* Increases the Ploidy in SPG Cells and Disrupts Septate Junctions. As SPG is an essential component of the *Drosophila* BBB (3, 4), we investigated whether SPG growth is mediated by *miR-285*. SPG nuclei were specifically labeled with GFP^{nls} driven by *moody-Gal4* (Fig. 3*A*). Much larger nuclei were detected in SPG cells in $miR\text{-}285^{KO}$ flies than in wild-type flies (Fig. 3 *A* and *B* and Fig. S4 *A* and *B*), and the nuclear size of SPG cells in $miR\text{-}285^{KO}$ flies was increased on average by ∼200% ($P < 0.001$; Fig. 3*E*), whereas expression of *miR-285* in SPG cells at 18 °C reduced the enlarged nuclear size in $miR\text{-}285^{KO}$ flies to the wild-type level ($P < 0.001$; Fig. 3 *D* and *E* and Fig. S4*D*). Conversely, overexpression of *miR-285* in SPG cells at 25 °C significantly reduced the nuclear size ($P < 0.001$; Fig. S2 *C* and *E* and Fig. S5*C*), even in $miR\text{-}285^{KO}$ flies (Fig. S2 *D* and *E* and Fig. S5*D*), to a nuclear size between that of *miR-285* overexpression and $miR\text{-}285^{KO}$ flies, suggesting an exquisite regulation of SPG growth by *miR-285*.

As the key function of SPG is to form septate junctions to ensure BBB integrity (5, 30), we further investigated whether septate junctions were defective in mutant flies with an abnormal nuclear size. Disrupted septate junctions were observed in 31% of brain samples from $miR\text{-}285^{KO}$ flies ($n = 32$) (Fig. 3*B′*), as shown by Discs Large (Dlg) staining, a component of septate junctions (31), a finding that is consistent with 30% of $miR\text{-}285^{KO}$ larval brains (n =30) displaying severe BBB defect in the dye penetration assay. At 18 °C, expression of *miR-285* driven by *moody-Gal4* caused a mild defect of septate junctions in 10% of flies ($n = 30$) (Fig. 3*C′*), whereas all brain samples with *miR-285* expression in $miR\text{-}285^{KO}$ flies ($n = 30$) (Fig. 3*D′*) showed morphologically normal septate junctions. On the other hand, overexpression of *miR-285* at 25 °C in either *WT* ($n = 15$) (Fig. S2*C′*) or $miR\text{-}285^{KO}$ flies ($n = 15$) (Fig. S2*D′*) resulted in disrupted septate junctions in all flies, a finding that is consistent with the results of the dye penetration assay (Fig. S2 *C″* and *D″*).

Cell size is invariably associated with the amount of DNA content and scaled to a large size with increased ploidy (10). A recent report suggested that SPG cells are polyploidy. The SPG cells use polyploidization to coordinate with the brain mass that is required for the maintenance of BBB (7). To investigate whether an aberrant nuclear size of SPG cells in $miR\text{-}285^{KO}$ flies is caused by an abnormal DNA content, SPG cells were labeled with RFP driven by *moody-Gal4* and were costained with the glial cell marker Repo. The DAPI intensity of individual SPG nuclei was measured and normalized against that of adjacent PG cells. The DNA content of SPG cells in $miR\text{-}285^{KO}$ flies (27.5 ± 9.6 C) was significantly increased on average by ∼165% compared with that in wild-type flies (15.9 ± 3.5 C) ($P < 0.001$; Fig. 3*F*), and the effect is fully rescued by the expression of *miR-285* at 18 °C (15.0 ± 3.2 C) (Fig. 3*F*). However, *miR-285* overexpression at 25 °C showed greatly reduced DNA content in either *WT* (9.3 ± 3.7 C) or $miR\text{-}285^{KO}$ flies (12.4 ± 3.5 C) (Fig. S2*F*), results that are consistent with the nuclear size under different genetic backgrounds (Fig. S2*E*). Moreover, along with increased ploidy in SPG cells, the brain lobe volume was increased in $miR\text{-}285^{KO}$ flies, whereas expression of *miR-285* suppressed brain overgrowth in $miR\text{-}285^{KO}$ flies (Fig. 3*G* and Fig. S2*G*). Thus, *miR-285* negatively regulates ploidy in SPG cells to restrict its nuclear size and brain volume during development.

Yki/Mask Works Downstream of *miR-285* to Maintain BBB Integrity in *Drosophila*. As *miR-285* is essential for BBB integrity and targets the Yki cofactor Mask, the Hippo signaling pathway might be required for the homeostasis of BBB. To prove this hypothesis, flies with *mask* knockdown or *yki* overexpression in SPG cells were generated. Similar to $miR\text{-}285^{KO}$ or *miR-285* overexpressed flies, *yki* overexpression at 25 °C (Fig. S6 *B′*, *B″*, *H*, and *J*) or *mask* knockdown by RNAi at both 18 °C (Fig. 4 *C′*, *C″*, *I*, and *K*) and 25 °C (Fig. S6 *D′*, *D″*, *H*, and *J*) led to abnormal SPG ploidy, nuclear size, disrupted septate junctions, and a BBB defect, suggesting an important role of the Hippo pathway in mediating BBB formation. The BBB defect in $miR\text{-}285^{KO}$ flies was almost fully rescued by the knockdown of *mask* in SPG cells at 18 °C or in flies heterozygous for the amorphic yki^{B5} allele at the L3 stage (Fig. 4 *D″* and *H″*), whereas the BBB defect was largely rescued when flies grow to adults (Fig. 4 *D‴* and *H‴*), suggesting that Mask is a downstream effector of *miR-285* to maintain BBB integrity.

To provide further evidence that Yki/Mask works downstream of *miR-285* to modulate SPG growth and BBB integrity, we examined SPG ploidy and nuclear size by manipulating Yki or Mask activities in SPG cells. The overexpression of *yki* in SPG cells significantly increased ploidy and nuclear size and reversed the reduction of SPG ploidy and nuclear size caused by *miR-285* overexpression at 25 °C (Figs. S6 *H* and *J* and S7 *B–B″* and *C–C″*). Additionally, knockdown of *mask* at 18 °C or $yki^{B5/+}$ heterozygosity almost fully rescued SPG ploidy and nuclear size of $miR\text{-}285^{KO}$ flies to the wild-type level (Fig. 4 *I* and *K* and Fig. S4 *F–F″* and *J–J″*). The brain hemisphere volume was coordinately changed with the ploidy and nuclear size of SPG cells (Fig. 4*J* and Fig. S6*I*). Thus, *miR-285*–Yki/Mask together constitute a signaling pathway to regulate the expression of downstream genes critical for the DNA content and size of SPG cells to maintain tissue size and function.

Abnormal Ploidy of SPG Cells in *miR-285* Mutant Occurs via *Cyclin E* Expression Level. It is known that cyclin E plays a pivotal role in regulating endoreplication, whereas continuously enforcing *cyclin E* expression stops endocycle in *Drosophila* (32) that is transcriptionally regulated by dE2F1. *Cyclin E* is also a target of Hippo pathway, and increased expression of cyclin E can be found in overgrowth tissues upon disruption of Hippo pathway (33). Our results have shown that Yki/Mask are essential to maintain the homeostasis of BBB downstream of *miR-285*, and we wished to know whether abnormal SPG ploidy in *miR-285* mutant occurs through the misregulated expression of *cyclin E*. Indeed, knockdown of *cyclin E* by RNAi at 18 °C suppressed the increased ploidy and nuclear size of SPG cells in $miR\text{-}285^{KO}$ mutant and almost fully rescued the defective septate junctions and BBB integrity (Fig. 4 *F′–F‴*, *I*, and *K*). Furthermore, knockdown of *cyclin E* at 25 °C significantly reduced ploidy and SPG size in both *WT* and $miR\text{-}285^{KO}$ flies and reversed the increased ploidy and SPG size caused by *miR-285* depletion (Figs. S6 *H* and *J* and S7 *F–F″* and *G–G″*), findings that are consistent with our suggestion that BBB integrity is maintained by an exquisite regulatory mechanism.

***miR-285*–Yki/Mask Forms a Feedback Loop to Modulate Hippo Signaling.** We have shown that Mask is a direct target of *miR-285* (Fig. 1 *A* and *D*), which positively regulates Yki activity and its downstream gene expression, including that of *cyclin E*, *diap1*, and *bantam* (17, 18). To further verify the role *miR-285* plays in regulating Yki activity, *bantam* expression was detected using a *GFP-bantam* sensor (BS-GFP in Fig. 5 *A′* and *A″*), which inversely reports *bantam* expression using the *bantam* targeting site constructed downstream of GFP in 3′UTR. Flp-out clones overexpressing *miR-285* in L3 brain or driven by *hh-Gal4* (DsRed in Fig. 5 *A–E* and Fig. S8 *A′–D′*) exhibited strong expression of BS-GFP (Fig. 5 *A′* and *A″* and Fig. S8 *A* and *A′*), suggesting decreased expression of *bantam*. Moreover, overexpression of *miR-285* reduced the expression of endogenous DIAP1, cyclin E (Fig. 5 *B′*, *B″*, *C′*, and *C″*), and *diap1-GFP* reporter (Fig. S8 *B* and *B′*). Reduced expression of endogenous DIAP1, cyclin E, and *diap1*-GFP can be reversed by coexpression of *yki* (Fig. 5 *D′*, *D″*, *E′*, and *E″* and Fig. S8 *D* and *D′*), and the reduced expression of *diap1*-GFP can be reversed by knockdown of *hpo* too (Fig. S8 *C* and *C′*). Furthermore, *miR-285*–depleted clones generated by MARCM showed up-regulated expression of DIAP1 (Fig. 5 *F–F″*) and cyclin E (Fig. 5 *G–G″*). Together, these results suggested that *miR-285* restricted Yki activity and repressed the expression of its downstream genes.

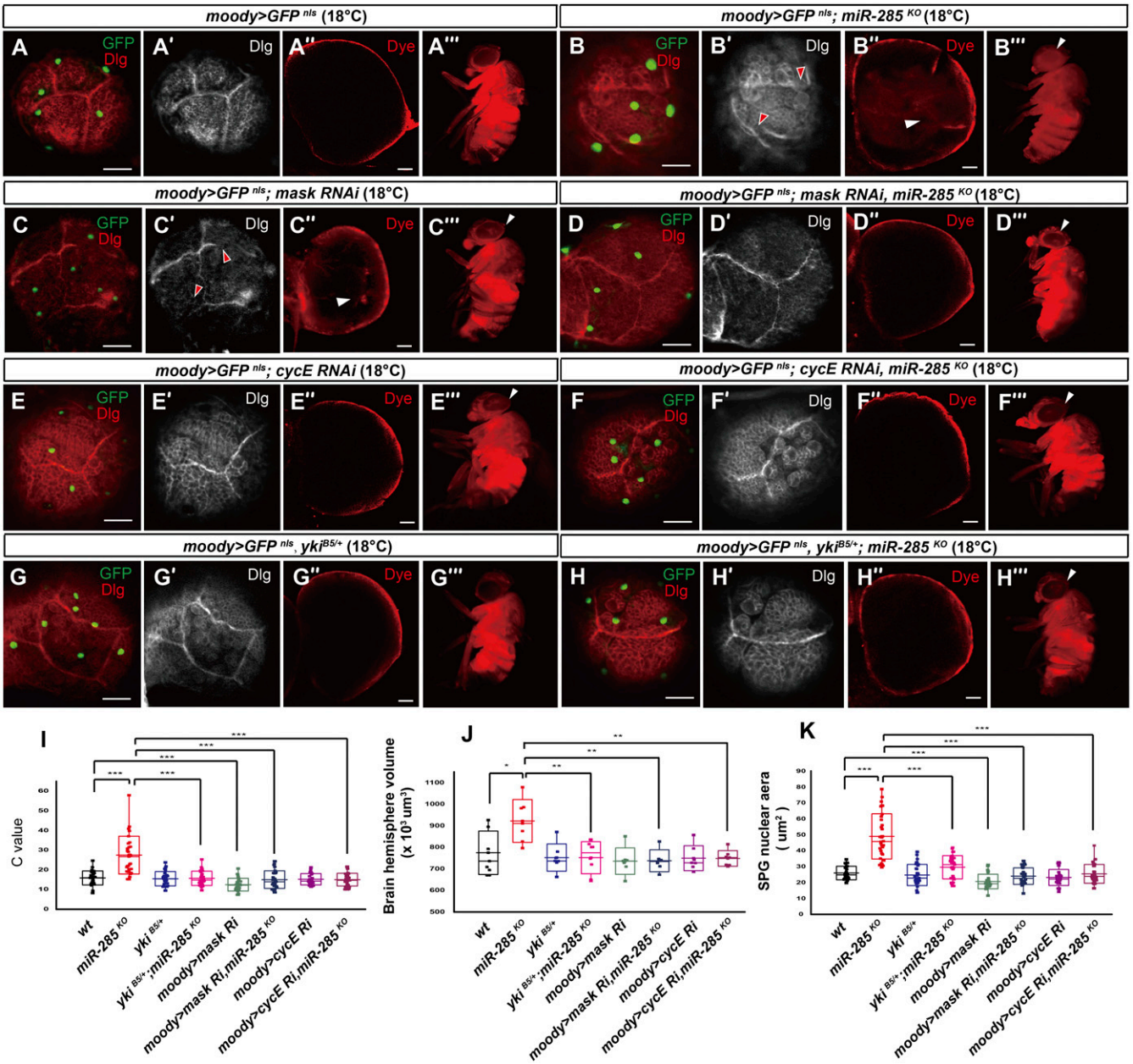

Fig. 4. Hippo pathway mediates SPG ploidy and BBB integrity. Third instar larval brain lobes were dissected from control (*A*); *miR-285*^{KO} (*B*); *moody* > *UAS-mask RNAi* (*C*); *moody* > *UAS-mask RNAi, miR-285*^{KO} (*D*); *moody* > *UAS-cycE RNAi* (*E*); *moody* > *UAS-cycE RNAi, miR-285*^{KO} (*F*); *yki*$^{B5/+}$ (*G*); and *yki*$^{B5/+}$*; miR-285*^{KO} (*H*) flies raised at 18 °C. SPG nuclei were labeled with *moody-Gal4* > *UAS-GFP*^{nls}, and the pattern of septate junctions was detected by Dlg antibody staining. The arrowheads indicate disrupted septate junctions and dye penetration. (*I*) Quantification of the polyploidy of indicated genotypes (SPG nuclei $n = 30$, from 10 larval brains). (*J*) Quantification of the brain hemisphere volume of indicated genotypes ($n = 7$). (*K*) Quantification of the SPG nuclei size of indicated genotypes (SPG nuclei $n = 30$, from 10 larval brains). The data shown are means ± SEM, and *P* value was noted as follows: **P* < 0.05, ***P* < 0.01, ****P* < 0.001. (Scale bar, 25 μm.)

Recent reports have shown that YAP/TAZ can modulate microRNA-processing enzymes Microprocessor or Dicer complexes and regulate the biogenesis of microRNAs in a cell density-dependent manner (20, 21); additionally, the microRNAs form gene regulatory networks (34). It is critical to know whether *miR-285* forms a feedback loop with Yki/Mask. We used the pan-glial driver *repo-Gal4* to drive gene expression in all glial cells and performed TaqMan quantitative PCR (qPCR) to measure *miR-285* expression under different backgrounds. Consistent with ISH data, *miR-285* expression was detected in *WT* larval brain and was undetectable in *miR-285*^{KO} flies (Fig. 5*H*), and elevated expression of *miR-285* was observed in *repo* > *miR-285* larval brain. Although overexpression of *yki* or knockdown of *hpo* significantly reduced the *miR-285* expression level, knockdown of *yki* or *mask* or overexpression of *yki* with *mask* knockdown exhibited an elevated *miR-285* expression (Fig. 5*H*). Together, these results suggested that *miR-285*–Yki/Mask forms a double-negative feedback loop to modulate Hippo signaling in larval brain.

Ectopic Expression of *miR-285* Induces Hippo Pathway-Mediated Apoptosis. The most known physiological functions of the Hippo signaling pathway are organ size control and tissue homeostasis, which are mainly due to well-balanced cell proliferation and apoptosis coordinated by YAP/Yki (35–37). We have shown

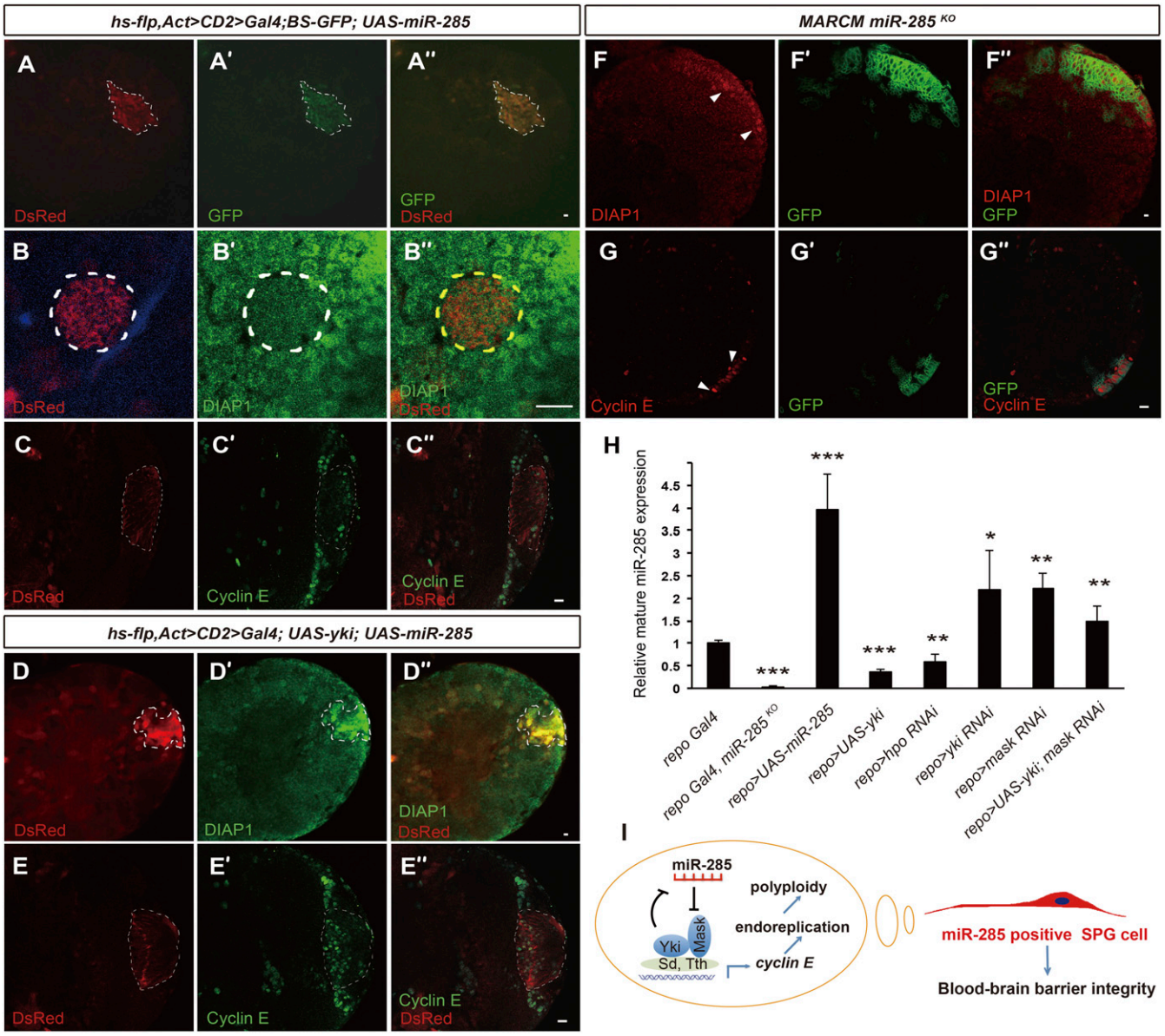

Fig. 5. *miR-285–Yki/Mask* double-negative feedback loop modulates Hippo signaling in larval brain. (*A–A′*) Flp-out clones expressing *miR-285* in the brain hemisphere from larval stage are marked by Dsred (red, *A*), with increased expression of *BS-GFP* (green, *A′*) and overlapping in white dashed circle (yellow, *A′′*). (*B–B′*) Flp-out clones expressing *miR-285* (red, *B*), with decreased expression of DIAP1 (green, *B′*) and overlapping in white dashed circle (yellow, *B′′*). (*C–C′*) Flp-out clones expressing *miR-285* (red, *C*), with decreased expression of cyclin E (green, *C′*) and overlapping in white dashed circle (yellow, *C′′*). (*D–D′′* and *E–E′*) Flp-out clones coexpressing *miR-285* (red, *D* and *E*) and *yki* in brain lobes from larval stage. Expression of *yki* reversed the reduced expression of DIAP1 (green, *D′* and *D′′*) and cyclin E (green, *E′* and *E′′*) caused by *miR-285* overexpression. (*F–F′′* and *G–G′′*) MARCM clones of *miR-285*^{KO} in brain lobes (GFP, *F′* and *G′*), stained with anti-DIAP1 (red, *F*) and anti-Cyclin E (red, *G*) antibodies, and overlapping (*F′′* and *G′′*). Mutant clones lacking *miR-285* exhibited elevated DIAP1 and cyclin E expression. (Scale bar, 5 μm.) (*H*) Yki inhibits *miR-285* expression. MicroRNA was extracted, and *miR-285* expression level was determined by quantitative RT-PCR. Experiments were performed in triplicate. The data shown are means ± SEM, and *P* value was noted as follows: **P* < 0.05, ***P* < 0.01, ****P* < 0.001. (*I*) Model of the *miR-285*–Yki/Mask regulatory mechanisms in regulating SPG cell ploidy and BBB integrity.

that *miR-285* regulates Yki activity and the expression of its downstream genes *cyclin E*, *bantam*, and *diap1*, which are required for cell proliferation and apoptosis, and we wished to know whether *miR-285* can regulate the proliferation–apoptosis balance by targeting Yki/Mask. Ectopically expressed *miR-285* was induced in developing eyes using *GMR-Gal4* (Fig. S9 *A* and *A′*) and in wings using *hh-Gal4* (Fig. S9 *B* and *B′*). The rough-eye (Fig. S10 *A* and *A′*) and smaller wrinkled wing (Fig. S10 *B* and *B′*) phenotypes were observed in *miR-285* overexpressed flies, respectively. These aberrant phenotypes could be caused by induced apoptosis associated with the inhibition of proliferation. We examined whether apoptosis was induced by overexpression of *miR-285* using anti-caspase 3 antibody staining. Spontaneous apoptosis was rarely observed in eye discs (Fig. S9*A*) or wing discs (Fig. S9*B*) in wild-type flies; however, substantial apoptosis was induced in both eye discs (Fig. S9*A′*) and wing discs (Fig. S9*B′*) when *miR-285* was overexpressed. Furthermore, the rough eye and small wing phenotype can be rescued by coexpression of antiapoptotic gene *p35* and deletion of one copy of the proapoptotic genes *hid*, *rpr*, and *grim* using *Df(H99)* or coexpression of *mask* (Fig. S10 *A–A′′′* and *B–B′′′′*); elevated apoptosis can also be eliminated (Fig. S10 *C–C′′′*). Thus, apoptosis caused by overexpression of *miR-285* occurs

through a canonical Hid–Reaper–Grim-promoted apoptotic pathway and requires caspases.

To decipher the functional link between *miR-285* and the Hippo signaling pathway in induced apoptosis, *hpo* knockdown or *yki* overexpression was generated along with *miR-285* overexpression. Induced apoptosis by *miR-285* overexpression was substantially reduced by *hpo* knockdown (Fig. S9 *E* and *E′*) and was completely eliminated by *yki* overexpression (Fig. S9 *F* and *F′*), suggesting that *miR-285* acts upstream of Yki to regulate cell growth. In addition, *mask* knockdown was similar to the overexpression of *miR-285* in both small eye phenotype and caspase activation (Fig. 1*E*” and Fig. S9*C′*). Moreover, *miR-285*–induced apoptosis is independent of p53 or JNK pathway, the two major apoptotic signaling pathways in *Drosophila* (38–40), because overexpression of *p53* intensified the rough eye phenotype induced by *miR-285* overexpression (Fig. S11 *A–C*), whereas loss of *p53* had no effect (Fig. S11 *E* and *F*), and a dominant-negative version of *Drosophila* JNK (bsk^{DN}) had no effect on either phenotype or caspase activation induced by *miR-285* overexpression (Fig. S11 *G–L*). Moreover, overexpression of *miR-285* or knockdown of *mask* in glial cells by *repo-Gal4* did not induce apoptosis (Fig. S12 *B* and *C*), and coexpression of *p35* could not rescue the defective BBB caused by *miR-285* overexpression (Fig. S12 *E* and *F*), indicating that the defective BBB caused by *miR-285* overexpression in SPG cells is not due to the increment of cell apoptosis, and a context-dependent regulatory mechanism exists to control cell growth through the *miR-285–Yki/Mask* signaling cascade.

Discussion

The regulation of cell growth and cell fate determination is central to tissue homeostasis. The Hippo signaling pathway is a key pathway to enable the dynamic regulation of tissue homeostasis during development. Although function and regulation of the Hippo pathway have been extensively studied, how Hippo signaling pathway is regulated remains incompletely understood in this important field. Since the first microRNA *lin-4* identified in *Caenorhabditis elegans*, the importance of microRNAs in regulation of various aspects of life and diseases has been well recognized; however, only very few microRNAs have been reported to mediate the growth control activity of Hippo pathway in vivo (24, 41). Recently, mammalian *miR-130a* was reported to amplify Yki signals through targeting its inhibitor VGLL4 and established a positive feedback loop (24). By investigating the well-known *bantam* in *Drosophila*, it was found that *bantam* functionally mimics mammalian *miR-130a* through targeting the Yki inhibitor SdBP/Tgi (24), although they do not share a conserved seed sequence. In this study, we identified a microRNA regulator, *miR-285*, of the Hippo pathway through genetic screening that directly targets Mask, a Yki coactivator essential for its transcriptional activity. Ectopic expression of *miR-285* suppresses the expression of Yki-targeted genes, inhibits cell proliferation, and induces apoptosis. More importantly, Yki suppresses the expression of *miR-285* and forms a *miR-285*–Yki/Mask double-negative feedback loop to modulate Hippo signaling toward downstream targets. Interestingly, *miR-285* targets Mask through noncanonical seed matching involving a G:U wobble without the 3′ compensatory pairing. The similar case of miRNA–mRNA recognition is reported in mammalian Nanog, which contains a functional wobble pairing site for *miR-296* without 3′ compensatory pairing (42). Other studies have also validated that targeting sites containing a single G:U base pair can function in vivo (43), and *let-7* recognizes *lin-41* with the wobble in seed sites (44), which need strong 3′ compensatory pairings. Notably, *miR-285* might be a *Drosophila* homolog of mammalian *miR-29* by seed sequence conservation (Fig. S13), and *miR-29* expression is regulated by YAP and mediates YAP targeting to PTEN to affect cell size (45), suggesting a conserved role of *miR-285* in controlling cell growth mediated by the Hippo pathway.

$miR\text{-}285^{KO}$ mutants grow normally, except that they have defective BBB integrity, indicating tissue-specific expression and functions of *miR-285*. Indeed, we detected highly expressed *miR-285* in larval brains. *Drosophila* BBB is primarily formed by SPG, constituting septate junctions to maintain the integrity of the BBB (46). To date, many factors, including Moody, Coiled, and Neurexin IV (26, 27, 47, 48), have been identified to mediate BBB formation. A recent report systemically identified *Drosophila* microRNAs essential to BBB integrity (25). However, whether microRNAs are required for SPG growth in *Drosophila* is unknown. The Merlin–Hippo signaling pathway was recently reported to regulate glial cell proliferation (15). As SPG cells do not proliferate after embryonic stage, the regulation of surface glial proliferation by the Merlin–Hippo pathway during larval stage should be mostly limited to the PG cells. However, whether the Hippo pathway is involved in the regulation of SPG cell growth and BBB integrity is still not known. Along with animals growing to a larger size, SPG cells increase their size through polyploidy to maintain a functional BBB instead of proliferation (7), whereas inhibition or increment of polyploidy in SPG cells causes the disruption of septate junctions and loss of barrier integrity.

Endoreplication is one of the major mechanisms by which polyploidy forms during development, and cyclin E/cdk2 is a central regulator of endoreplication in *Drosophila*. *Cyclin E* is transcribed before the onset of endocycle S phase and is required for these cycles, and ectopic expression of *cyclin E* triggers precocious DNA replication in endoreplicating tissues (30). Although the control of *cyclin E* transcription via E2F is believed to be a cornerstone of G1/S cell-cycle progression, *cyclin E* gene also responds directly to the Hippo signaling pathway, which often occurs when developmental programs coordinate cell-cycle progression with cell differentiation (31). On the other hand, Yki/Sd could coordinate with dE2F1 to induce a specific transcriptional program necessary to bypass cell-cycle exit (49), suggesting a complex cross-talk between the Hippo and Rb/E2F pathways during development. Our findings suggested that during development, a well-balanced *cyclin E* expression is critical to modulate the DNA content in SPG cells by regulating Yki activity. Improperly increased or decreased activity of Yki leads to dysregulated cyclin E expression, irregular SPG ploidy, and disrupted BBB integrity. It would be interesting to explore the potential interlink between *miR-285*–Yki/Mask and dE2F in regulating cyclin E expression in endoreplicating tissues during development.

Due to its critical roles during development, dysregulation of the Hippo signaling pathway has been involved in several diseases, including cancer and cardiovascular and neurodegenerative diseases (16, 50–54), and it was recently reported that Mask modulates the morphology of mitochondria and negatively regulates Parkin recruitment to mitochondria (55). The maintenance of the BBB is critical for neuronal functions, and its breakdown will alter the transport of molecules between blood and brain and may also result in progressive synaptic and neuronal dysfunction and loss in disorders such as Alzheimer's disease and Parkinson's disease (56–59). Our findings provide insights into the mechanistic link between the elaborate regulation of Hippo signaling and BBB functions and may also shed light on the relationship between neurodegenerative disorders and dysregulation of Hippo signaling and BBB. Therefore, Hippo signaling might become a potential therapeutic target for targeted therapy approaches in selected patient populations with BBB disorders. In summary, we demonstrated exquisite regulation of ploidy in SPG cells and the maintenance of a functional BBB during development through the *miR-285*–Yki/Mask double-negative feedback loop. It will be interesting to know whether this function is conserved in higher eukaryotes and to test its relevance to tissue homeostasis in different contexts.

Materials and Methods

Fly Genetics. All flies were maintained at 18 °C or 25 °C on standard corn meal unless specified. Fly lines used in this study were as follows: w^{1118}; *hh-Gal4*; *en-Gal4*; *ey-Gal4*; *repo-Gal4*; *GMR-Gal4*; *moody-Gal4* (gift from Margaret Ho, Tongji University School of Medicine, Shanghai, China); $UAS\text{-}GFP^{nls}$; *UAS-RFP*;

TI{TI}miR-285^{KO}; *UAS-bsk^{DN}*; *UAS-p35*; *Df(H99)*; *Df(3L)Exel6115*; *Df(3L)BSC458*; *Df(3L)BSC840*; *UAS-DsRed-miR-285* (gift from Eric C. Lai, Memorial Sloan Kettering Cancer Center, New York); *yki^{B5}*; *bantam sensor* (gift from Stephen M. Cohen, University of Copenhagen, Copenhagen); *UAS-yki* and *diap1-GFP* (gifts from Lei Zhang, Shanghai Institute of Biochemistry and Cell Biology, Chinese Academy of Sciences, Shanghai); and *UAS-mask* (gift from Chunlai Wu, Louisiana State University Health Sciences Center, New Orleans). *UAS-cycE RNAi*; *UAS-mask RNAi* were obtained from the Tsing Hua Fly Center (THFC).

Fly Genotyping. The genotyping of *miR-285^{KO}* flies was performed by PCR. The following PCR primers were used: 285 (WT) forward (F), 5′-CAAAAGCACTGATTTCGAATGG-3′ and 285 (WT) reverse (R), 5′-TGAGTGGATCTGACATCGCACC-3′; and 285 (KO) F, 5′-TTTGACACTTCGCTGGCGG-3′ and 285 (KO) R, 5′-GCTTAGACTCTTCGGTGTCCATTAC-3′.

Clonal Analysis. Flp-out clones were induced 48 h after egg laying (AEL) in staged larvae by 37 °C heat shock for 60 min. The larval genotypes were as follows: *hs-flp, act > CD2 > Gal4/UAS-DsRed-miR-285* and *hs-flp, act > CD2 > Gal4/UAS-yki; UAS-DsRed-miR-285*. Flp-out clones were marked by Dsred. For MARCM clonal analysis, the clones were induced 48 h AEL by a 60 min, 37 °C heat shock. The genotypes used were as follows: *yw, hs-flp*; *UAS-GFP*; and *tubGal4, FRT82B, tubGal80/FRT82B, miR-285^{KO}*.

Generation of Anti-DIAP1 Antibody. Full-length *diap1* cDNA was cloned into the protein expression vector pET28a (Novagen), and protein expression was induced in BL21-competent cells. The gel slice corresponding to DIAP1 fusion protein was cut, crushed, emulsified with Freund's adjuvant, and injected into rabbits (Abgent) to generate anti-DIAP1 antibody. Sera were collected over a period of 2 mo and were purified by affinity purification.

Histology and Imaging. The brains, wing discs, and eye discs from third instar larvae of the desired genotypes were dissected in cold PBS and were immediately fixed in PBS containing 4% (wt/vol) paraformaldehyde. The samples were washed with PBT (PBS containing 0.2% Triton X-100) three times, blocked in PBTB [PBT containing 5% (vol/vol) normal goat serum], and incubated with primary antibodies overnight. The following primary antibodies were used: rabbit anti-cleaved Caspase 3 (Cell Signaling Technology 9661L, 1:400), mouse anti-Repo (Developmental Studies Hybridoma Bank 8D12, 1:50), mouse anti-Dlg (Developmental Studies Hybridoma Bank 4F3, 1:50), goat anti-Cyclin E (Santa Cruz sc-15903, 1:200), and rabbit anti-DIAP1 (1:200). After three washes with PBT, secondary anti-mouse (Cell Signaling Technology, 1:400), anti-goat (Life Technologies, 1:400), or anti-rabbit (Cell Signaling Technology, 1:400) fluorescence antibodies, including Alexa 488 and 555, were used. Samples were mounted and analyzed on a Leica SP5 and Olympus FV1000 confocal laser-scanning microscope. Adult wing and eye images were obtained using a Nikon SMZ1500 microscope. The images were processed using Adobe Photoshop, Illustrator, and ImageJ.

ISH. Locked nucleic acid (LNA)-probe ISH was performed as previously described (60) using an *miR-285* probe (labeled at both 5′ and 3′ ends with DIG) from Exiqon (33035-15), which was used for hybridization at 42 °C.

Dye Penetration Assay. Dye penetration experiments were performed as previously described (26). Ten kDa Texas red-conjugated dextran solution (2.5 mM; Life Technologies D-1863) was injected into the body cavity of third instar larvae or adults at 5–7 d old. Flies were allowed to recover in fresh vials for 16–24 h. Larval brains were dissected and analyzed under a Leica SP5 confocal laser-scanning microscope. Dye penetration into the adult retina was examined under an Olympus SZX16 fluorescence microscope.

miRNA–mRNA 3′UTR Alignment. The binding site of *miR-285* in *mask* 3′UTR was analyzed using miRanda (www.microrna.org/microrna/) and Targetscan (www.targetscan.org).

Constructs and Transgenes. The Actin5C-promoter DNA fragment from pAC5.1 vector (Life Technologies) was inserted into pGL3-basic plasmid (Promega) to generate Actin5C-firefly luciferase plasmid. The pAC5.1-renilla luciferase plasmid was constructed by cloning renilla luciferase from pRL-TK (Promega) into pAC5.1 vector. A 2,234-bp fragment of full-length *mask* 3′UTR was amplified by PCR from wild-type genomic DNA and was cloned downstream of firefly luciferase in the Actin5C-firefly luciferase plasmid. Mutated *mask* 3′UTR was generated by mutagenesis of the complementary *miR-285* seed sequence from "TGGTGTT" to "ACTGCAG." A 439-bp fragment spanning *miR-285* gene locus was amplified by PCR using primers F, 5′-CCGCTCGAGAAGACCCGGTCAACGAGATG-3′ and R, 5′-TCCCCGCGGCCTAAACAGAGGTCGCGCCTGT-3′ and was cloned into pAC5.1 vector for *miR-285* expression.

The 3′UTR constructs were generated by cloning the full-length 3′UTR of *Drosophila mask*, *ex*, and *sd* genes into the 3′ end of the tub-GFP reporter vector (61). Transgenic flies were generated by standard procedures.

Luciferase Reporter Assays. *Drosophila* Schneider S2 cells were cultured in SFX-Insect Media (HyClone) and were cotransfected with 100 ng of firefly luciferase reporter plasmid carrying wild-type *mask* 3′UTR or mutated *mask* 3′UTR and 200 ng of pAC5.1-miR-285 or empty pAC5.1 plasmid DNA in 24-well plates. The cells were also cotransfected with 50 ng of pAC5.1-renilla luciferase plasmid DNA for normalization. The relative luciferase activity was measured 60 h posttransfection using the Dual-Glo Luciferase Assay system (Promega).

RNA Isolation and Real-Time PCR. MicroRNA was extracted from third instar larval brains using the mirVana miRNA isolation kit (Life Technologies). The relative expression level of *miR-285* was determined using Taqman microRNA Assays (Life Technologies) and was normalized to RNU6B.

Image Analysis. ImageJ software was used to quantify the nuclear size and DNA content. Repo staining was used to mark SPG and PG nuclei. An area was drawn and measured around the target nuclei on each optical section (Z stack) after deconvolution. The area function was used to obtain SPG nuclear area. The DNA amount was quantified by DAPI intensity, and ploidy was calculated by normalizing each SPG nucleus to nearby Repo-positive diploid PG cells imaged on the same slide with the same settings. The brain lobe volume was measured using Volocity 3D analysis software (PerkinElmer), where optimized standard measurement protocols were applied to all control and experimental samples for each dataset.

Statistics. All statistical comparisons were performed using origin 9.0. The *P* values were calculated using a two-sample *t* test. The significance levels were indicated as follows: $*P < 0.05$, $**P < 0.01$, and $***P < 0.001$. Sample sizes were indicated in the figure legends and *Results*.

ACKNOWLEDGMENTS. We thank Drs. Margaret Ho, Eric C. Lai, Stephen M. Cohen, Lei Zhang, Chunlai Wu, Core Facility of Drosophila Resource and Technique, Shanghai Institute of Biochemistry and Cell Biology, Chinese Academy of Sciences, Tsing Hua Fly Center, and Bloomington Stock Center for fly stocks; laboratory of Changjiang Scholar at Dalian Medical University for help with confocal microscopy; and members of the X.B. and Z.Y. laboratories for advice and discussions. This work was supported by National Natural Science Foundation of China Grants 31271480 and 31501165 and the Hundred Talent program of the Chinese Academy of Sciences, a Pandeng scholarship of Liaoning province, and Qizhen Gongcheng from Dalian Medical University (to X.B.).

1. Zhao Z, Nelson AR, Betsholtz C, Zlokovic BV (2015) Establishment and dysfunction of the blood-brain barrier. *Cell* 163(5):1064–1078.
2. Obermeier B, Daneman R, Ransohoff RM (2013) Development, maintenance and disruption of the blood-brain barrier. *Nat Med* 19(12):1584–1596.
3. Hindle SJ, Bainton RJ (2014) Barrier mechanisms in the Drosophila blood-brain barrier. *Front Neurosci* 8:414.
4. Limmer S, Weiler A, Volkenhoff A, Babatz F, Klämbt C (2014) The Drosophila blood-brain barrier: Development and function of a glial endothelium. *Front Neurosci* 8:365.
5. Stork T, et al. (2008) Organization and function of the blood-brain barrier in Drosophila. *J Neurosci* 28(3):587–597.
6. Awasaki T, Lai SL, Ito K, Lee T (2008) Organization and postembryonic development of glial cells in the adult central brain of Drosophila. *J Neurosci* 28(51):13742–13753.
7. Unhavaithaya Y, Orr-Weaver TL (2012) Polyploidization of glia in neural development links tissue growth to blood-brain barrier integrity. *Genes Dev* 26(1):31–36.
8. Orr-Weaver TL (2015) When bigger is better: The role of polyploidy in organogenesis. *Trends Genet* 31(6):307–315.
9. Otto SP (2007) The evolutionary consequences of polyploidy. *Cell* 131(3):452–462.
10. Schoenfelder KP, Fox DT (2015) The expanding implications of polyploidy. *J Cell Biol* 209(4):485–491.
11. Chow BW, Gu C (2015) The molecular constituents of the blood-brain barrier. *Trends Neurosci* 38(10):598–608.
12. Rangarajan R, Courvoisier H, Gaul U (2001) Dpp and Hedgehog mediate neuron-glia interactions in Drosophila eye development by promoting the proliferation and motility of subretinal glia. *Mech Dev* 108(1-2):93–103.
13. Witte HT, Jeibmann A, Klämbt C, Paulus W (2009) Modeling glioma growth and invasion in Drosophila melanogaster. *Neoplasia* 11(9):882–888.
14. Read RD, Cavenee WK, Furnari FB, Thomas JB (2009) A drosophila model for EGFR-Ras and PI3K-dependent human glioma. *PLoS Genet* 5(2):e1000374.
15. Reddy BV, Irvine KD (2011) Regulation of Drosophila glial cell proliferation by Merlin-Hippo signaling. *Development* 138(23):5201–5212.
16. Yu FX, Zhao B, Guan KL (2015) Hippo pathway in organ size control, tissue homeostasis, and cancer. *Cell* 163(4):811–828.

17. Sidor CM, Brain R, Thompson BJ (2013) Mask proteins are cofactors of Yorkie/YAP in the Hippo pathway. *Curr Biol* 23(3):223–228.
18. Sansores-Garcia L, et al. (2013) Mask is required for the activity of the Hippo pathway effector Yki/YAP. *Curr Biol* 23(3):229–235.
19. Oh H, Irvine KD (2010) Yorkie: The final destination of Hippo signaling. *Trends Cell Biol* 20(7):410–417.
20. Mori M, et al. (2014) Hippo signaling regulates microprocessor and links cell-density-dependent miRNA biogenesis to cancer. *Cell* 156(5):893–906.
21. Chaulk SG, Lattanzi VJ, Hiemer SE, Fahlman RP, Varelas X (2014) The Hippo pathway effectors TAZ/YAP regulate dicer expression and microRNA biogenesis through Let-7. *J Biol Chem* 289(4):1886–1891.
22. Thompson BJ, Cohen SM (2006) The Hippo pathway regulates the bantam microRNA to control cell proliferation and apoptosis in Drosophila. *Cell* 126(4):767–774.
23. Nolo R, Morrison CM, Tao C, Zhang X, Halder G (2006) The bantam microRNA is a target of the hippo tumor-suppressor pathway. *Curr Biol* 16(19):1895–1904.
24. Shen S, et al. (2015) A miR-130a-YAP positive feedback loop promotes organ size and tumorigenesis. *Cell Res* 25(9):997–1012.
25. Chen YW, et al. (2014) Systematic study of Drosophila microRNA functions using a collection of targeted knockout mutations. *Dev Cell* 31(6):784–800.
26. Bainton RJ, et al. (2005) moody encodes two GPCRs that regulate cocaine behaviors and blood-brain barrier permeability in Drosophila. *Cell* 123(1):145–156.
27. Schwabe T, Bainton RJ, Fetter RD, Heberlein U, Gaul U (2005) GPCR signaling is required for blood-brain barrier formation in drosophila. *Cell* 123(1):133–144.
28. Duffy JB (2002) GAL4 system in Drosophila: A fly geneticist's Swiss army knife. *Genesis* 34(1-2):1–15.
29. Katzenberger RJ, et al. (2015) Death following traumatic brain injury in Drosophila is associated with intestinal barrier dysfunction. *eLife* 4:4.
30. Hatan M, Shinder V, Israeli D, Schnorrer F, Volk T (2011) The Drosophila blood brain barrier is maintained by GPCR-dependent dynamic actin structures. *J Cell Biol* 192(2): 307–319.
31. Woods DF, Bryant PJ (1991) The discs-large tumor suppressor gene of Drosophila encodes a guanylate kinase homolog localized at septate junctions. *Cell* 66(3):451–464.
32. Edgar BA, Orr-Weaver TL (2001) Endoreplication cell cycles: More for less. *Cell* 105(3): 297–306.
33. Duronio RJ, Xiong Y (2013) Signaling pathways that control cell proliferation. *Cold Spring Harb Perspect Biol* 5(3):a008904.
34. Herranz H, Cohen SM (2010) MicroRNAs and gene regulatory networks: Managing the impact of noise in biological systems. *Genes Dev* 24(13):1339–1344.
35. Hansen CG, Moroishi T, Guan KL (2015) YAP and TAZ: A nexus for Hippo signaling and beyond. *Trends Cell Biol* 25(9):499–513.
36. Varelas X (2014) The Hippo pathway effectors TAZ and YAP in development, homeostasis and disease. *Development* 141(8):1614–1626.
37. Aqeilan RI (2013) Hippo signaling: To die or not to die. *Cell Death Differ* 20(10): 1287–1288.
38. Mollereau B, Ma D (2014) The p53 control of apoptosis and proliferation: Lessons from Drosophila. *Apoptosis* 19(10):1421–1429.
39. Biteau B, Karpac J, Hwangbo D, Jasper H (2011) Regulation of Drosophila lifespan by JNK signaling. *Exp Gerontol* 46(5):349–354.
40. Shlevkov E, Morata G (2012) A dp53/JNK-dependent feedback amplification loop is essential for the apoptotic response to stress in Drosophila. *Cell Death Differ* 19(3): 451–460.
41. Lin CW, et al. (2013) MicroRNA-135b promotes lung cancer metastasis by regulating multiple targets in the Hippo pathway and LZTS1. *Nat Commun* 4:1877.
42. Tay Y, Zhang J, Thomson AM, Lim B, Rigoutsos I (2008) MicroRNAs to Nanog, Oct4 and Sox2 coding regions modulate embryonic stem cell differentiation. *Nature* 455(7216): 1124–1128.
43. Brennecke J, Stark A, Russell RB, Cohen SM (2005) Principles of microRNA-target recognition. *PLoS Biol* 3(3):e85.
44. Vella MC, Choi EY, Lin SY, Reinert K, Slack FJ (2004) The C. elegans microRNA let-7 binds to imperfect let-7 complementary sites from the lin-41 3'UTR. *Genes Dev* 18(2): 132–137.
45. Tumaneng K, et al. (2012) YAP mediates crosstalk between the Hippo and PI(3)K–TOR pathways by suppressing PTEN via miR-29. *Nat Cell Biol* 14(12):1322–1329.
46. Alvarez JI, Katayama T, Prat A (2013) Glial influence on the blood brain barrier. *Glia* 61(12):1939–1958.
47. Nilton A, et al. (2010) Crooked, coiled and crimpled are three Ly6-like proteins required for proper localization of septate junction components. *Development* 137(14): 2427–2437.
48. Baumgartner S, et al. (1996) A Drosophila neurexin is required for septate junction and blood-nerve barrier formation and function. *Cell* 87(6):1059–1068.
49. Nicolay BN, Bayarmagnai B, Islam AB, Lopez-Bigas N, Frolov MV (2011) Cooperation between dE2F1 and Yki/Sd defines a distinct transcriptional program necessary to bypass cell cycle exit. *Genes Dev* 25(4):323–335.
50. Gomez M, Gomez V, Hergovich A (2014) The Hippo pathway in disease and therapy: Cancer and beyond. *Clin Transl Med* 3:22.
51. Heallen T, et al. (2011) Hippo pathway inhibits Wnt signaling to restrain cardiomyocyte proliferation and heart size. *Science* 332(6028):458–461.
52. von Gise A, et al. (2012) YAP1, the nuclear target of Hippo signaling, stimulates heart growth through cardiomyocyte proliferation but not hypertrophy. *Proc Natl Acad Sci USA* 109(7):2394–2399.
53. Lee JK, et al. (2013) MST1 functions as a key modulator of neurodegeneration in a mouse model of ALS. *Proc Natl Acad Sci USA* 110(29):12066–12071.
54. Orcholski ME, Zhang Q, Bredesen DE (2011) Signaling via amyloid precursor-like proteins APLP1 and APLP2. *J Alzheimers Dis* 23(4):689–699.
55. Zhu M, Li X, Tian X, Wu C (2015) Mask loss-of-function rescues mitochondrial impairment and muscle degeneration of Drosophila pink1 and parkin mutants. *Hum Mol Genet* 24(11):3272–3285.
56. Sagare A, et al. (2007) Clearance of amyloid-beta by circulating lipoprotein receptors. *Nat Med* 13(9):1029–1031.
57. Matsumoto Y, et al. (2007) Blood-brain barrier permeability correlates with medial temporal lobe atrophy but not with amyloid-beta protein transport across the blood-brain barrier in Alzheimer's disease. *Dement Geriatr Cogn Disord* 23(4):241–245.
58. Drożdzik M, et al. (2003) Polymorphism in the P-glycoprotein drug transporter MDR1 gene: A possible link between environmental and genetic factors in Parkinson's disease. *Pharmacogenetics* 13(5):259–263.
59. Lee CG, et al. (2004) MDR1, the blood-brain barrier transporter, is associated with Parkinson's disease in ethnic Chinese. *J Med Genet* 41(5):e60.
60. Vallejo DM, Caparros E, Dominguez M (2011) Targeting Notch signalling by the conserved miR-8/200 microRNA family in development and cancer cells. *EMBO J* 30(4): 756–769.
61. Gao L, et al. (2013) Drosophila miR-932 modulates hedgehog signaling by targeting its co-receptor Brother of ihog. *Dev Biol* 377(1):166–176.